Continental Shelf Research 226 (2021) 104490

Contents lists available at ScienceDirect

Continental Shelf Research

journal homepage: www.elsevier.com/locate/csr

Seasonal variability of upwelling and downwelling surface current patterns in a small coastal embayment

Nicholas Trautman, Ryan K. Walter *

Physics Department, California Polytechnic State University, San Luis Obispo, CA, USA

ARTICLE INFO

Keywords:
High frequency radar
Coastal upwelling
Upwelling seasonality
Upwelling bay
Upwelling jet
Upwelling shadow

ABSTRACT

Upwelling in coastal embayments is important to a variety of physical and biological processes. Despite their ubiquity, circulation patterns in small bays (width and length scales $\leq$ 20 km) in eastern boundary current upwelling systems are relatively understudied compared to their larger counterparts. In this study, we apply a conditional averaging technique to investigate upwelling- and downwelling-driven circulation in a small coastal embayment located in Central California (San Luis Obispo Bay). We also investigate intraseasonal differences in the current patterns. Conditional averaging reveals distinct intraseasonal differences and features that are obscured by traditional seasonal averages when examining the upwelling jet separation and onshore advection, horizontal divergence patterns, and particle trajectories. We show that the upwelling circulation and resulting upwelling jet separation and onshore advection reinforce a convergent upwelling shadow front at this site, with important ecological ramifications. While tuned specifically for San Luis Obispo Bay, these findings can be used as a baseline for similar small upwelling bays, highlight the importance of conditional averages (versus traditional temporal averages), and underline the importance of coastal upwelling seasonality beyond the common bimodal upwelling and non-upwelling description.

1. Introduction

Coastal embayments are common coastal features whose morphology and orientation can produce complex spatial patterns in local and regional surface currents (Largier 2020). For the past several decades, oceanographers have observed these surface patterns using high-frequency radar (HF radar or HFR), a technique which makes use of Bragg scattering and the Doppler effect to determine the velocity of surface currents from reflected HF radio waves (Paduan and Washburn 2013). Surface currents in coastal embayments often form complex spatial patterns of significant ecological importance which can be studied using HFR-derived measurements of the current field. Many ecologically important processes are mediated by surface current patterns including the development, fate, and transport of harmful algal blooms (HABs) (Matson et al., 2019); frontogenesis and localized upwelling (Walter et al., 2017); the dispersal of buoyant plumes (Coulliette et al., 2007; Warrick et al., 2007; Kim et al., 2009); and larval dispersal and connectivity (Zelenke et al., 2009; Nidzieko and Largier 2013), the latter of which is especially important to the design and assessment of marine protected areas.

In eastern boundary current systems, coastal upwelling is the dominant driver of variability, and along with topography and coastline orientation, helps shape the complex surface patterns observed near embayments (i.e., "upwelling bays," cf. Largier 2020). Coastal topography and shoreline changes near bays significantly affect local upwelling intensity by altering alongshore wind patterns through blocking, deflecting, and/or accelerating the winds (see Largier 2020 and the references therein). Coastal headlands upstream of embayments are also regions of enhanced upwelling (i.e., upwelling center) and can block or deflect the shelf jet, often leading to an upwelling jet that separates from the coast before either reattaching, following isobaths along-shore, curving cyclonically, or some combination of these (see Largier 2020 and the references therein). In small bays (defined here as having width and length scales that are 20 km or less, but still greater that the local baroclinic Rossby radius of deformation, cf. Largier 2020), limited prior observations have identified a range of complex circulation patterns, but many of these observations were from short-duration shipboard surveys that did not capture temporal variability (either seasonally or synoptically) of upwelling wind forcing, or a limited number of moorings that could not capture small-scale spatial variability (Valle-Levinson et al.,

* Corresponding author.
E-mail address: rkwalter@calpoly.edu (R.K. Walter).

https://doi.org/10.1016/j.csr.2021.104490
Received 24 February 2021; Received in revised form 25 June 2021; Accepted 6 July 2021
Available online 8 July 2021

2000, 2004; Roughan et al., 2005a, 2005b; Moraga-Opazo et al., 2011; Largier 2020 and the references therein). Given the limited observations, there is a need for an improved understanding of circulation patterns in small upwelling bays.

Coastal upwelling forcing in eastern boundary current systems exhibits marked seasonality (Checkley and Barth, 2009; Garcia-Reyes and Largier, 2012; Walter et al., 2018). Thus, it is important to understand how these seasonal changes in upwelling modify surface circulation patterns and features, particularly in small upwelling embayments. Paduan et al. (2018) investigated typical upwelling-driven current patterns in Monterey Bay, a large coastal embayment (length and width scales much greater than 20 km) located in Central California. They compared traditional averages of surface current patterns over the summer upwelling season and winter non-upwelling season to those averaged conditionally during upwelling and downwelling events to isolate upwelling circulation patterns. They found that conditional averages resulted in significantly more structure and intensity in the current patterns, with important implications for predicting dynamically and ecologically relevant features in the region. Here, we apply the conditional averaging technique of Paduan et al. (2018) to investigate the upwelling-driven circulation in a small coastal embayment located in Central California [San Luis Obispo (SLO) Bay]. We also investigate the intra-upwelling season variability by examining the oceanic response to both traditional and conditional averages using a more detailed description of upwelling seasonality (Walter et al., 2018, see Section 2.1) that goes beyond the common bimodal description of upwelling and non-upwelling seasons. Horizontal divergence patterns and particle trajectories under the various scenarios are also explored to help highlight some of the dynamical and ecological implications of the findings.

2. Data and methods

2.1. SLO bay study site

SLO Bay is a small (~2 km wide in the northern portion) and shallow (~10 m average depth) embayment on the California Central Coast located approximately 80 km north of Pt. Conception, a major marine biogeographical boundary (Fig. 1). SLO Bay features a vast ecological diversity including giant kelp forests, a major local fishing port (Port San Luis), and several popular beach destinations. The embayment is defined by both Pt. Buchon and Pt. San Luis headlands to the northwest, which partially shelter the bay, and Pt. Sal to the south (Fig. 1b). During the upwelling season, these headlands shelter the northern portion of the bay from prevailing upwelling winds, leading to increased retention and warmer surface waters in the bay that are distinct from cold, recently upwelled waters in the upwelling jet outside the bay (Walter et al., 2018). Like other so-called upwelling shadow front systems, SLO Bay experiences periods of high stratification and high phytoplankton biomass (Walter et al. 2017, 2018), and it is prone to HABs (Barth et al., 2020) and hypoxia (Valera et al., 2020). This study is the first investigation of seasonal surface current patterns in this ecologically important region.

2.2. Upwelling seasonality

While coastal upwelling is traditionally considered a bimodal process (i.e., the summer upwelling season and the winter non-upwelling season), this generalized framework does not capture details relevant to marine ecosystems (Garcia-Reyes and Largier 2012; Walter et al., 2018). Using both the mean monthly upwelling favorable wind stress and the monthly standard deviation, Walter et al. (2018) presented a tuning of the annual cycle and a more detailed description of the upwelling seasonality for the SLO Bay region. They refined the commonly described upwelling season to highlight significant intraseasonal variability including a Peak Upwelling season (April and May) and Upwelling Relaxation season (July, August, and September), and the non-upwelling season to a Winter Transition season (October and November) and Winter Storms season (December, January, and February), with March and June considered "upwelling transition periods." The Peak Upwelling season (April and May) is characterized by the largest mean upwelling-favorable winds, although they are also highly variable due to the frequent wind relaxations. This season is also characterized by the presence of cold, nutrient rich waters, and an increase in chlorophyll concentrations throughout the water column. During the Upwelling Relaxation season (July to September), the mean upwelling winds decrease significantly with less variability, and water-column stratification intensifies while chlorophyll concentrations remain elevated near the surface. During the full upwelling season (March to September), major upwelling events typically have time scales on the order of a few days to weeks and are followed by wind relaxation events. The conditional averaging technique applied here (Section 2.5) isolates and captures the upwelling-driven circulation component during major events. During the Winter Transition season (October and November), the mean upwelling winds continue to decrease until they reach their minimum during the Winter Storms season (December to February), although by this time the monthly variability increases substantially due to synoptic (i.e., storm-driven) variability. During this time, vertical temperature and chlorophyll gradients start to erode due to increased vertical mixing, and the distribution becomes more uniform vertically with minimum chlorophyll concentrations. A more detailed description of this intraseasonal variability and the oceanic response can be found in Walter et al. (2018).

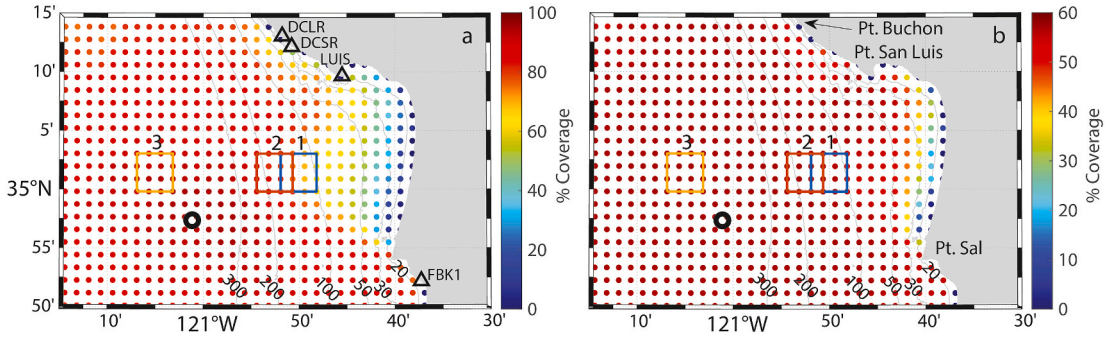

Fig. 1. (a) Percent coverage of HFR data from October 1, 2011 to December 31, 2019 across the SLO Bay domain. (b) Percent coverage across the domain when restricting to times when at least 90% of all spatial points have data available. The boxes labeled 1, 2, and 3 are the subregions used to calculate the spin-up time (see Section 2.5). Representative isobaths (in m) are also shown (gray lines) and labeled (black, bottom). The locations of HFR sites (triangles, panel a), NDBC Buoy #46011 (circle, both panels), and points/headlands referenced in the paper (panel b) are shown.

2.3. Surface current data

Hourly 2 km resolution HFR measurements of the surface current velocity field from October 1, 2011 to December 31, 2019 were downloaded from the UCSD THREDDS data server (https://hfrnet-tds.ucsd.edu/thredds/catalog.html) within the region bounded by 121.25°W to 120.5°W and 34.83°N to 35.25°N (Fig. 1). The percent coverage of HFR data in the domain is shown in Fig. 1. Times when the spatial coverage throughout the domain was less than 90% were excluded from further analysis (Fig. 1b; see also Fig. 2 for times that were excluded). Since the focus of this analysis is on the upwelling- and downwelling-driven circulation, a low-pass filter (33 h) was applied to the data following Paduan et al. (2018) in order to eliminate strong tidal flows and diurnal-wind driven currents in this region (e.g., Walter et al., 2017) that may not be completely removed with the ensemble conditional averaging described below.

2.4. Offshore wind data

To assess regional wind-driven upwelling, hourly offshore winds were obtained from the National Data Buoy Center (NDBC) Buoy #46011 (Fig. 1a, ~ 35 km offshore of SLO Bay). Equatorward upwelling favorable winds were calculated using the local coastline orientation (150° from true north; Fig. 1a, cf. Walter et al., 2018) such that positive quantities denote upwelling favorable and negative indicate downwelling favorable. These winds were also filtered using a low-pass filter (33 h) following Paduan et al. (2018). In order to pair upwelling winds with HFR velocities, the timestamps of the filtered winds were interpolated onto those of the filtered surface currents (see Fig. 2). Upwelling events were then defined as periods when upwelling winds exceeded 5 m/s for at least 48 h and downwelling or relaxation events as periods when upwelling winds were less than −3 m/s for at least 24 h (Figs. 2 and 3), following Paduan et al. (2018).

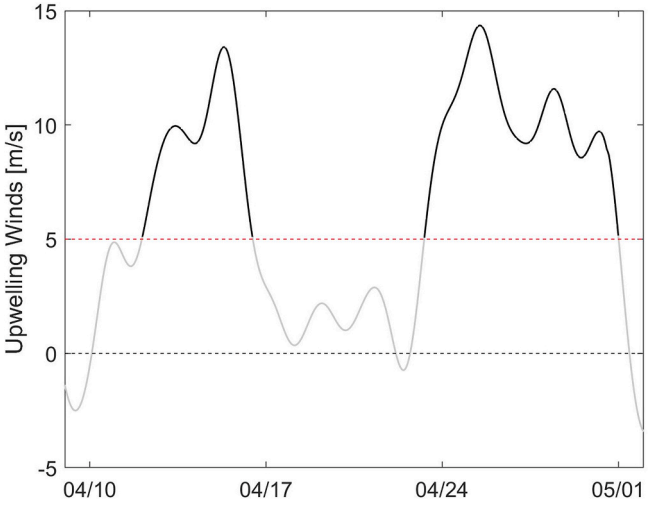

Fig. 3. Example time series of upwelling favorable winds from April 2016 (Peak Upwelling season). Upwelling events are defined as periods when the upwelling winds exceeded 5 m/s (red dashed line) for at least 48 h. (For interpretation of the references to color in this figure legend, the reader is referred to the Web version of this article.)

2.5. Conditional averaging process and spin-up times

Upwelling conditional averages were calculated for the Peak Upwelling (April and May) and Upwelling Relaxation (July to September) seasons, as well as the full upwelling season from March to September (Table 1). Downwelling conditional averages were calculated for the Winter Transition (October and November) and Winter Storm (December to February) seasons, as well as the full non-upwelling season (October to February) (Table 1). For comparison, the traditional average for each of the aforementioned time periods was also calculated. Additionally, the horizontal divergence of the flow field and frozen field flow

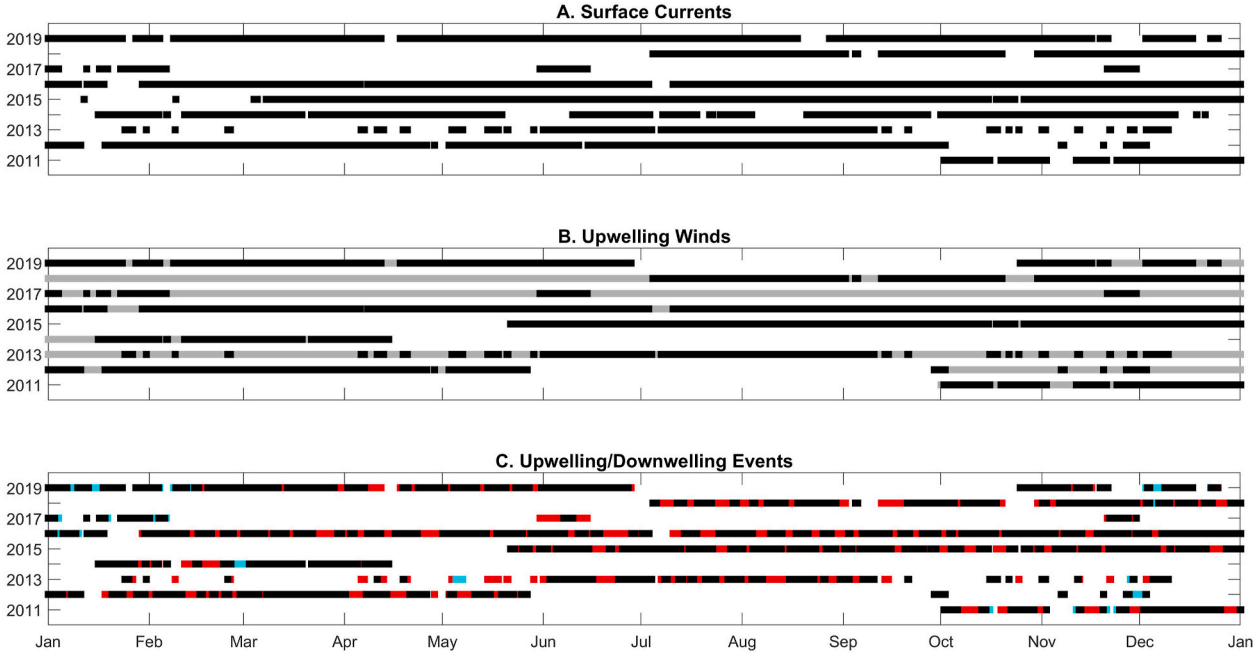

Fig. 2. Temporal coverage of (a) HFR-derived surface current velocity, (b) upwelling winds, and (c) upwelling/downwelling events. In (a), only times where the spatial coverage throughout the domain was greater than 90% are shown. In (b), times where wind data are available are shown in gray and times where both wind and current data are available in black. (c) Times when upwelling favorable winds exceed 5 m/s (red, upwelling events) or are less than −3 m/s (cyan, downwelling events) are superimposed on the times corresponding to overlapping wind and current availability (black) from (b). Year labels are shown every other year. (For interpretation of the references to color in this figure legend, the reader is referred to the Web version of this article.)

Table 1
Number of events used to compute conditional averages.

Season		Number of Upwelling Events
Upwelling	Upwelling (March–September)	81
	Peak Upwelling (April–May)	20
	Upwelling Relaxation (July–September)	44
Number of Downwelling Events		
Non-upwelling	Non-upwelling (October–February)	23
	Winter Transition (October–November)	10
	Winter Storms (December–February)	13

trajectories for traditional and conditional averages for each season were also computed. Divergence values along the coast were excluded due to the lack of data availability and uncertainty in the estimates (Fig. 1). Frozen flow field trajectories were computed by placing particles at an initial spatial position and advecting the particle's position using a fourth-order Runge Kutta scheme and the fixed (i.e., traditional or conditional average), interpolated velocity field at each hourly time step for up to 14 days, or more commonly until the particle advects outside of the HFR grid (typically within a few days).

In order to determine the spin-up time required to reach a quasi-steady state for the conditional averages, the average kinetic energy of different subregions (i.e., the points in boxes 1–3 in Fig. 1) was computed as a function of the time since the start of an upwelling event over all upwelling events, following Paduan et al. (2018) (Fig. 4). The approximate time required to reach a steady state was 2 days. The kinetic energy remained at a quasi-steady state, and there were a sufficient number of events to compute a representative average, until approximately six days after the start of an upwelling event. The conditional averages for upwelling were further refined by including only times within this two-to six-day range. Downwelling events were conditionally averaged over the first three days of an event. Major results and conditionally averaged current patterns were not significantly influenced by small changes to the conditional averaging windows and spin-up times.

3. Results

3.1. Upwelling circulation patterns

3.1.1. Full upwelling season (March to September)

The traditionally and conditionally averaged surface current fields for the full upwelling season (March to September) are shown in Fig. 5a and b, respectively. In both cases, an upwelling jet is visible across the mouth of the bay and advects towards the shore near the southern end of the bay. The upwelling jet is somewhat more prominent in the conditionally averaged current field compared to the traditionally averaged field. In Fig. 5c and d, a region of strong convergence can be observed where waters from inside the northern region of the bay meet the upwelling jet. There is also a strong nearshore divergence zone at the southern end of the upwelling jet where some currents advect onshore and others continue south. This divergence is slightly amplified in the conditionally averaged current field, a result of the enhanced magnitude of the upwelling jet and its shoreward advection. Fig. 5e and f shows similar particle trajectories in both the traditional and conditional averages. More particles are entrained in the upwelling jet in the conditional average, highlighting the potential for greater retention in the bay.

3.1.2. Peak Upwelling season (April and May)

For the Peak Upwelling season (April and May), the upwelling jet is an even more prominent feature in both the traditional and conditional averages compared to the full upwelling season (Fig. 6a and b). However, it is stronger in the conditional average, especially in the nearshore. The divergence pattern is similar for both the traditional and conditional average (Fig. 6c and d). The magnitude of the nearshore divergence is increased in the conditional average, which corresponds to the more defined southern boundary of the upwelling jet observed in the conditionally averaged current field. This augmented divergence corresponds to a stronger, southward flow that separates from the

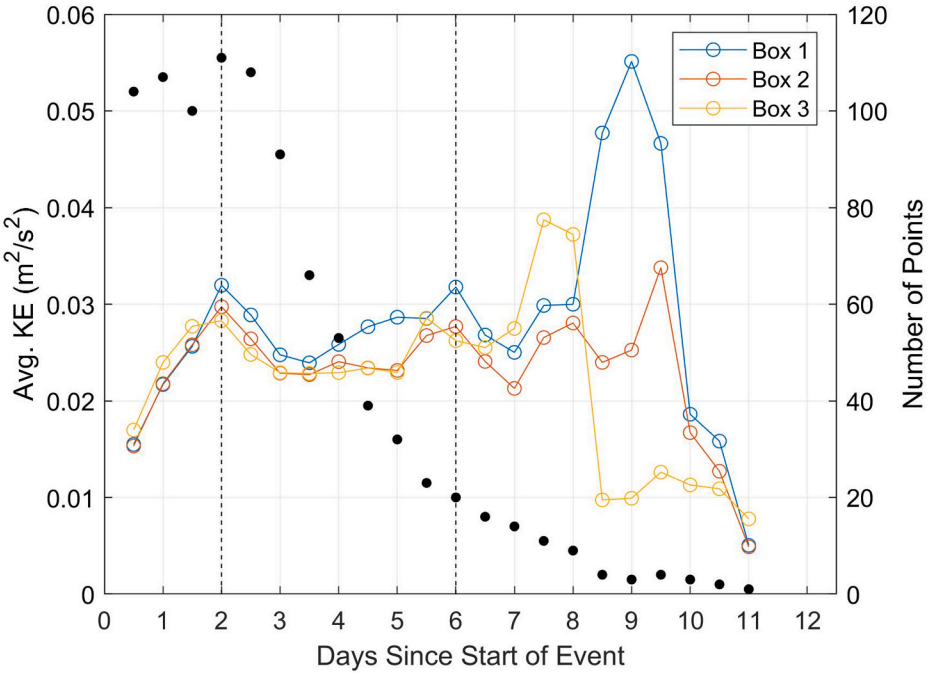

Fig. 4. Average kinetic energy (left axis) of the subregions in Fig. 2 calculated in days since the start of an upwelling event (upwelling winds > 5/m/s). Shown with vertical dashed lines is the quasi-steady state period over which conditional averages are calculated (i.e., 2–6 days), where the kinetic energy has remained quasi-steady and there are a sufficient number of events (right axis) for the conditional averages.

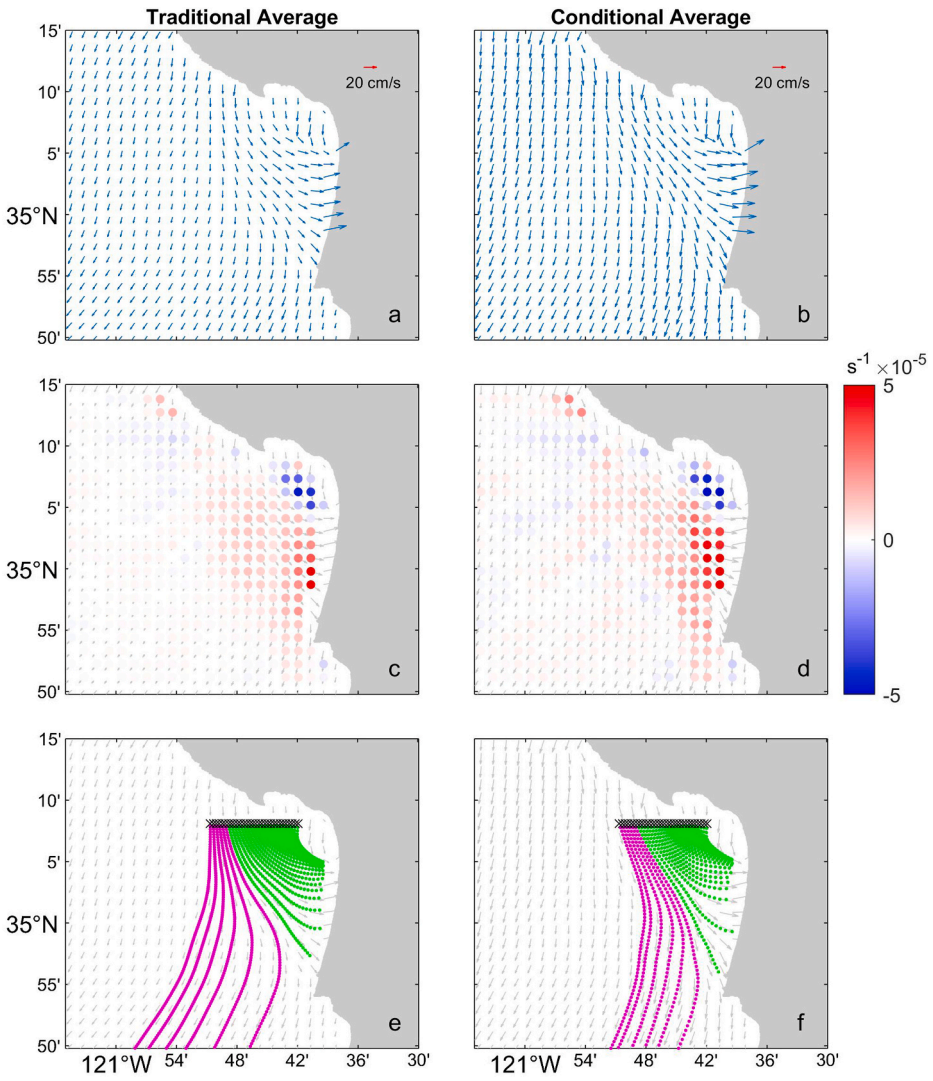

Fig. 5. (a, b) Traditional and conditional averages (upwelling events) of surface current data for the full upwelling season (March to September). (c, d) Horizontal divergence patterns overlaying the averaged current fields. (e, f) Frozen flow field particle trajectories overlaying the averaged current fields. For comparison, the green trajectories in both (e, f) correspond to particles advected into SLO Bay by the traditionally averaged flow field, while magenta trajectories do not advect into the bay by the traditionally averaged flow field. The release points of the particles are indicated by a black "x". For all panels, the traditionally averaged quantities are on the left, while the conditionally averaged quantities are on the right. Each particle's position was updated every hour for 14 days, or more commonly until the particle advects outside of the HFR grid (typically within a few days). (For interpretation of the references to color in this figure legend, the reader is referred to the Web version of this article.)

upwelling jet sooner than in the traditional average (6a, 6b). While the particle trajectories shown in Fig. 6e and f are generally similar, retention of waters within the bay is diminished in the conditional average, as the increased strength of the upwelling jet and nearshore divergence zone results in the advection of a greater number of particles past the bay.

3.1.3. *Upwelling Relaxation season (July to September)*

In both the traditional and conditional averages for the Upwelling Relaxation season (July to September), the upwelling jet is still visible, but reduced in magnitude. In general, the strength of the current field is diminished compared to the Peak Upwelling season and the upwelling season in its entirety (Fig. 7a and b). The jet is, however, amplified in the conditional average in the Upwelling Relaxation season, as are the magnitudes of the currents. In Fig. 7c and d, the nearshore divergence is significantly enhanced in the conditional average compared to the traditional average, as is the convergence in the northern region of SLO Bay. This is the most noticeable difference in divergence patterns observed for any of the upwelling seasons investigated. In the particle trajectories (Fig. 7e and f), this manifests as a pronounced split just north of Pt. Sal (southern end of SLO Bay, see Fig. 1b) between the waters retained within the bay and those advected past it to the south. For comparison, the traditionally averaged trajectories fan out and displace more uniformly from their release points at a slower rate. There is also a significant westward component to these trajectories which is present in the conditional average, but absent in the Peak Upwelling Season and full upwelling season trajectories. This westward velocity component leads to reduced retention of particles within the bay compared to the other upwelling seasons and is one of the more prominent intraseasonal differences observed. Generally, it should also be noted that both the traditional and conditional averages for the entire upwelling season are influenced more by the Peak Upwelling season averages (Fig. 6) than the Upwelling Relaxation season averages (Fig. 7).

3.2. *Downwelling circulation patterns*

3.2.1. *Full non-upwelling season (October to February)*

Whereas the traditionally averaged current field is reminiscent of that of the Upwelling Relaxation season (Fig. 7a), the most prominent feature of the full non-upwelling season (October to February) is the reversal of the currents in the conditional average (Fig. 8a and b). In the conditional average, the upwelling jet is no longer present and the currents inside and outside of the bay are poleward (Fig. 8b). The nearshore poleward flow is strongest near Pt. Buchon, with weaker poleward advection along the outer edge of SLO Bay. The traditionally and conditionally averaged divergence fields both display a very weak nearshore divergence zone near the southern end of the bay (Fig. 8c and d). There is also a region of convergence near Pt. Buchon, which corresponds to the strong poleward flow visible in Fig. 8b. The traditionally averaged particle trajectories (Fig. 8e) are similar to those of the

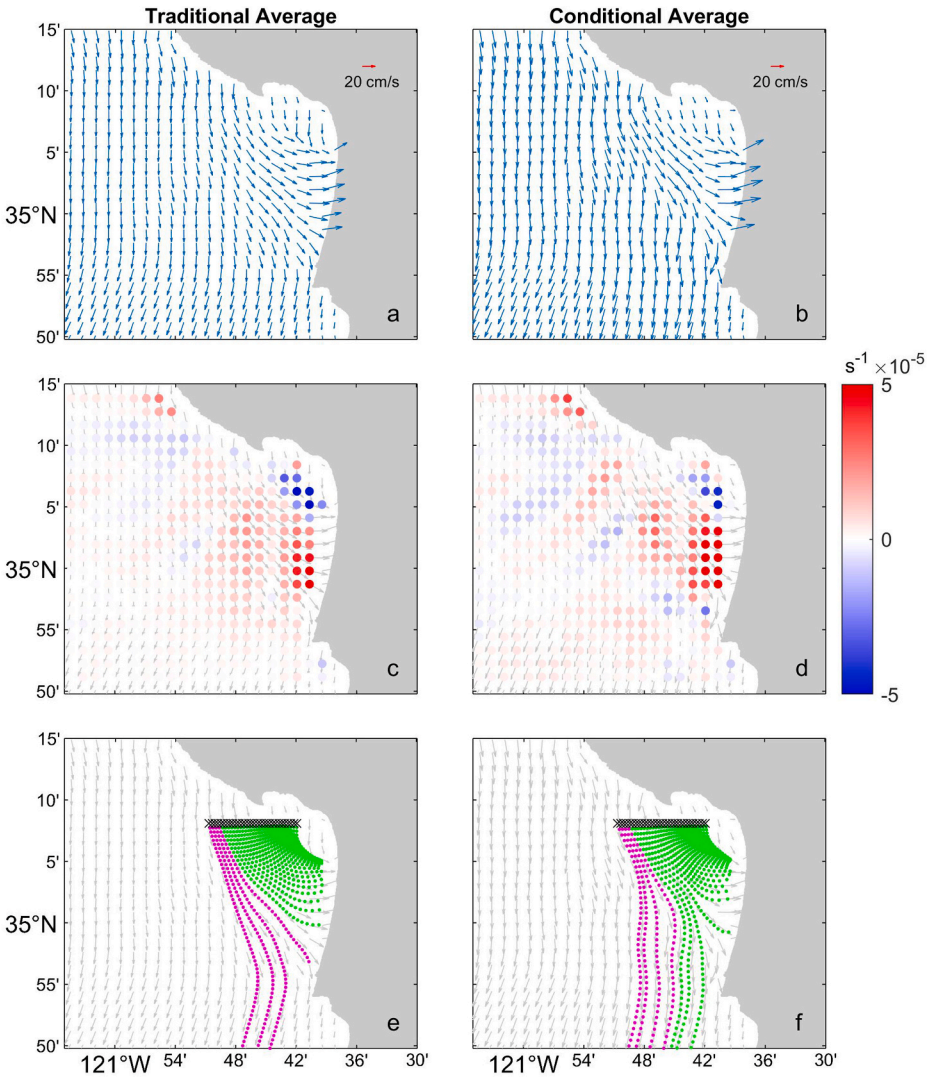

Fig. 6. Same as Fig. 5, but for the Peak Upwelling season (April and May).

Upwelling Relaxation season (Fig. 7e), but with reduced magnitude and a greater westward component. Since the direction of the flow is reversed in the conditional average, particles were released off of Pt. Sal instead of in the northern region of the bay (Fig. 8f). The conditionally averaged trajectories show a prominent flow separation just outside the southern end of SLO Bay with some particles retained within the bay and the rest advected northward. It appears that retention in the bay is reduced in the conditional average, but due to the flow reversal, it is more difficult to compare the traditionally and conditionally averaged trajectories and retention.

3.2.2. *Winter Transition season (October and November)*

The general structure of the traditionally and conditionally averaged current fields for the Winter Transition season (October and November) is similar to that of the non-upwelling season as a whole (Fig. 9a and b). The traditional average displays a weak westward flow, whereas the conditional average shows a northward flow that is weak within the bay but intensifies as it nears Pt. Buchon to the north. As in the entire non-upwelling season, this intensified flow corresponds to a zone of relatively strong convergence in the conditional average, which is not present in the traditional average (Fig. 9c and d). For the traditional average, the degree of retention in the bay is very low, as most of the surface currents advect westward out of the bay (Fig. 9e).

3.2.3. *Winter Storms season (December to February)*

For the Winter Storms season (December to February), while there is some semblance of an upwelling jet and onshore advection in the traditionally averaged current field, it is significantly weaker than in the upwelling seasons (Fig. 10a). The conditionally averaged currents show the expected poleward flow near Pt. Buchon, which is stronger here than in the Winter Transition season (Fig. 10b). Similar to the divergence zone that forms near Pt. Sal during the upwelling seasons, there is a modest increase in the strength of the divergence in the traditional average (Fig. 10c). There is also a region of increased convergence near Pt. Buchon as was observed for the Winter Transition season and the entire non-upwelling season (Fig. 10d). The traditionally averaged particle trajectories support the observation of a weak current field, although there is a strong degree of retention in the northern portion of SLO Bay (Fig. 10e). This contrasts with the conditionally averaged trajectories, in which there is no retention whatsoever as the particles that enter the bay after passing through the Pt. Sal divergence zone eventually exit after reaching a convergence zone in the middle of the bay (Fig. 10f).

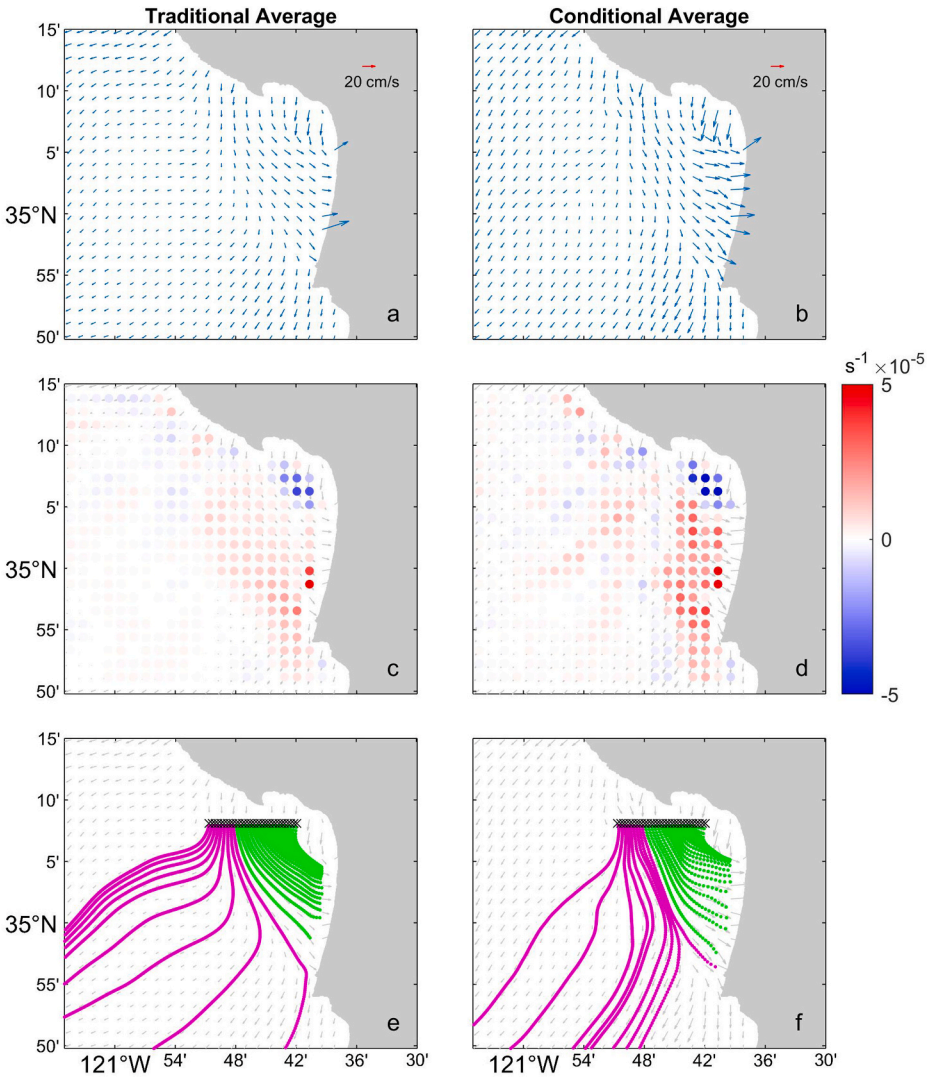

Fig. 7. Same as Fig. 5, but for the Upwelling Relaxation season (July, August, and September).

4. Discussion

4.1. Upwelling seasonality

The seasonality of coastal upwelling has long been established, with many studies considering a summer upwelling season and a winter non-upwelling season. Taking a conditional average of the HFR-derived surface current field based on upwelling-favorable winds reveals patterns that are obscured by a traditional average of these seasons (Paduan et al., 2018). Moreover, we show that applying the same conditional averaging with the more detailed seasonality proposed by Walter et al. (2018), which documents significant intraseasonal variability in both the upwelling and non-upwelling seasons, additional current patterns and features are revealed.

In comparing the results of Paduan et al. (2018) to those of this study, it is important to note the morphological differences between Monterey Bay and SLO Bay. While both bays are flanked by upwind and downwind headlands, Monterey Bay is several times larger than SLO Bay and has a width and length that are closer to one another ("square bay"), whereas the width of SLO Bay is greater than twice its length ("wide-open bay") (Largier 2020). Paduan et al. (2018) showed that for upwelling events that reached quasi-steady state, a strong cyclonic flow developed within Monterey Bay and a pronounced, southward-flowing jet formed across the mouth. In SLO Bay, a similar upwelling jet can be seen in the conditionally averaged current field for the broader upwelling season, along with significant onshore advection (Fig. 5). In Monterey Bay, the seasonal and conditional averages computed were significantly different in all cases considered, but in SLO Bay, the differences were comparably less pronounced during upwelling events compared to downwelling events. This suggests that there is relatively much more current variability, including reversals, in Monterey Bay during strong upwelling forcing. In SLO Bay, a full cyclonic eddy does not develop during upwelling, presumably due to the geometry of the bay. The coastal topography (upstream and downstream headlands and their characteristics), the size of the embayment, and local bathymetry are likely important in inhibiting the formation of a fully-developed eddy (Largier 2020). Nonetheless, there are still important differences between traditional averages and conditional averages for both upwelling and downwelling events in SLO Bay.

Examination of the current patterns for the upwelling season as defined in Walter et al. (2018) revealed that upwelling events occurring in the Peak Upwelling season appeared to contribute more to the spatial patterns observed in the full upwelling season than upwelling events occurring during the Upwelling Relaxation season. During the full non-upwelling season, a strong poleward flow developed in both Monterey Bay and SLO Bay. Interestingly, there was much less intraseasonal variation for downwelling events, with the main difference being that the flow intensified during the Winter Storms season compared to the

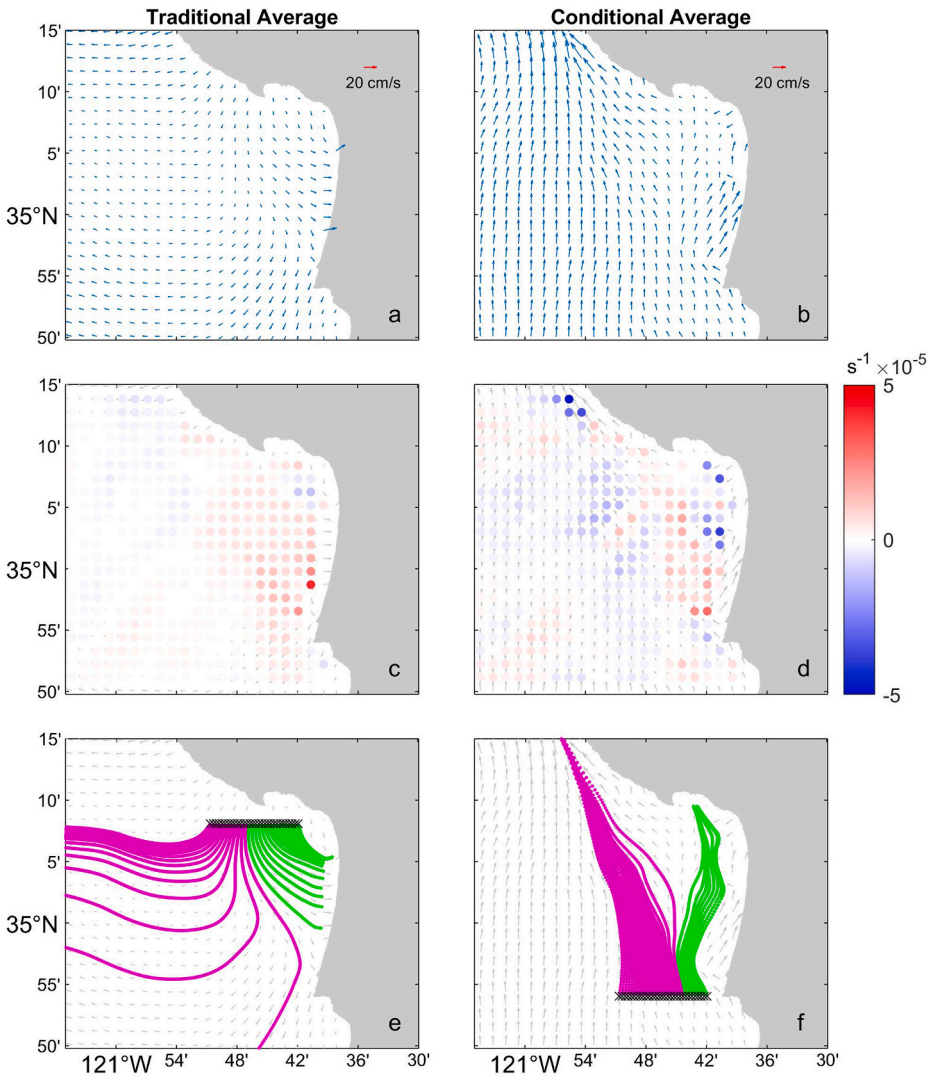

Fig. 8. Same as Fig. 5, but for the non-upwelling season (October to February) and downwelling events. For the conditionally averaged frozen flow field in (e, f), particles are released near Pt. Sal instead of in the northern region of SLO Bay, due to the predominantly northward currents. Particle trajectories for both averages are colored based on whether or not the particles advect into the bay (green) or not (magenta). (For interpretation of the references to color in this figure legend, the reader is referred to the Web version of this article.)

Winter Transition season and the full downwelling season. While there were marked differences in the traditionally and conditionally averaged flow fields during the upwelling season, the most substantial differences were observed during downwelling events when equatorward flows in the traditional averages switched to poleward flows in the conditional averages. The intraseasonal differences observed during the full upwelling season, as well as the strong differences between traditionally averaged flow fields versus conditionally averaged ones during both upwelling and downwelling forcing, highlight the importance of upwelling seasonality in determining local circulation patterns.

4.2. *Upwelling dynamics in small upwelling shadow embayments*

Small embayments (length and width scales $\leq$ 20 km) are ubiquitous in eastern boundary current upwelling systems, comprising just under 40% of all the bays classified by a recent review of upwelling bays (Largier 2020). Of these, roughly 70% are classified as being dominated by either an upwelling shadow or upwelling trap. Despite their ubiquity, these bays are understudied, with limited prior observations coming from short-duration shipboard surveys that did not capture temporal variability (either seasonally or synoptically), or a limited number of moorings that could not capture small-scale spatial variability (Valle-Levinson et al., 2000, 2004; Roughan et al., 2005a, 2005b; Moraga-Opazo et al., 2011; Largier 2020 and the references therein). Thus, the results here could serve as a baseline for understanding, interpreting, and predicting seasonal circulation patterns, as well as upwelling- and downwelling-driven circulation, in other small upwelling bays with similar features.

The results presented here also provide further evidence for the development and reinforcement of an upwelling shadow in the northern region of SLO Bay (cf. Walter et al., 2018). During the upwelling season, a marked thermal gradient develops between the warm waters in the bay (upwelling shadow) and the cold waters in the upwelling jet outside the bay (Fig. 11). This thermal gradient corresponds to the same region of enhanced convergence observed across the mouth of the bay during the full upwelling, Peak Upwelling, and Upwelling Relaxation seasons. During upwelling, this convergent front acts as a barrier to bay-shelf exchange, promoting retention and a warmer surface layer in the upwelling shadow inside the bay. In turn, this acts to increase the cross-front baroclinic pressure gradient force, reinforcing the convergence region along the thermal front. These frontal systems are maintained for days to weeks until the next upwelling wind relaxation event, although some upwelling shadow bays have been shown to exceed the timescale of synoptic upwelling-relaxation cycle variability (Largier 2020). The frontal convergence region is enhanced during the Upwelling Relaxation season relative to the Peak Upwelling season, which is corroborated by long-term cross-front temperature measurements (see Fig. 10 in Walter et al., 2018). Moreover, the convergence across the mouth is significantly enhanced in the conditionally averaged flow field compared to the traditionally averaged field during the Upwelling

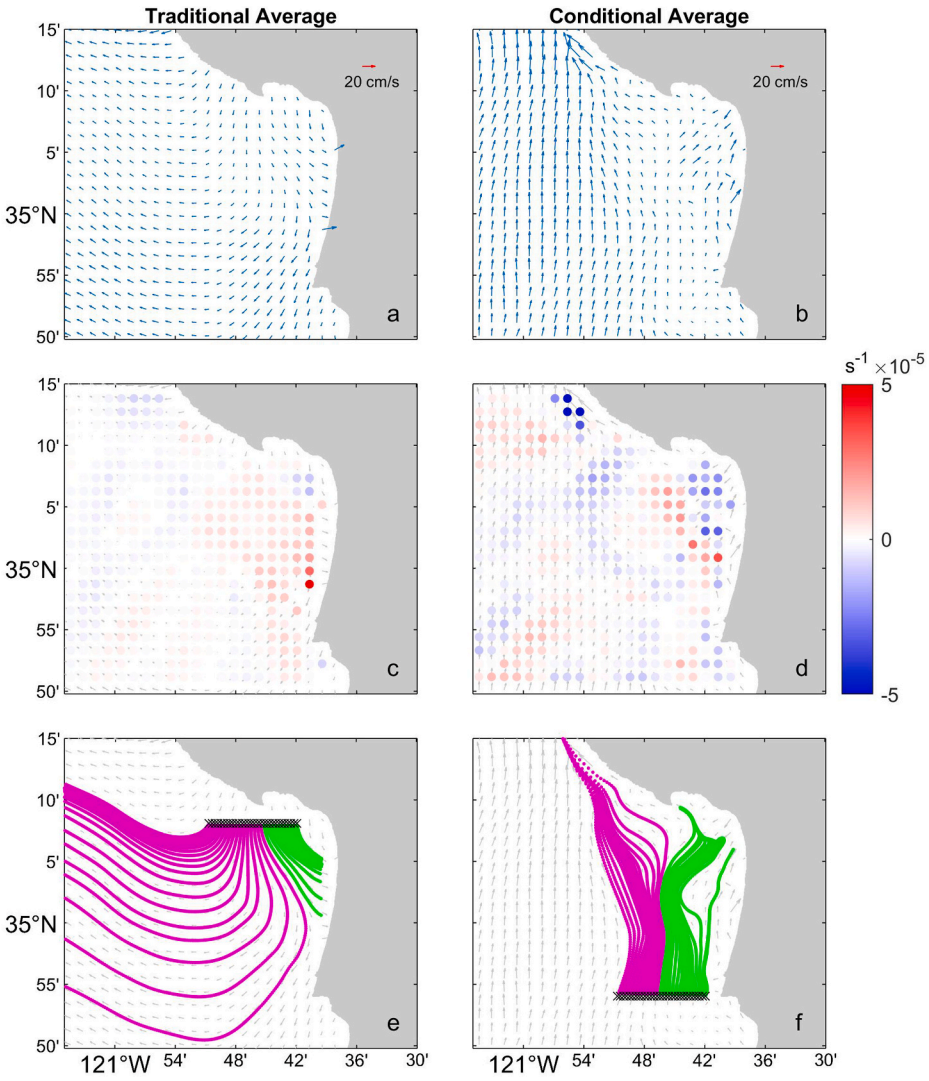

Fig. 9. Same as Fig. 8, but for the Winter Transition season (October and November).

Relaxation season. These convergent upwelling fronts can also be modulated by local diurnal wind forcing (Woodson et al. 2007, 2009; Walter et al., 2017) and are sites of increased internal wave activity (Walter et al., 2016). These results highlight the importance of intra-seasonal upwelling variability and upwelling-driven circulation to dynamically relevant features in small upwelling embayments.

A full dynamical analysis is beyond the scope of this study, particularly with the limitations imposed with only surface current data, but some insight can be gained by generally considering the shelf jet forcing, wind forcing, and thermal forcing during upwelling [see framework presented in Largier (2020)]. These terms can be scaled as U^2/L, $\tau/\rho H$, and $g'H/L$, respectively, where U is the shelf jet velocity scale, L is the bay length scale, H is the bay depth, scale, τ is the upwelling wind stress, ρ is water density, and g' is the reduced gravity determined from bay-ocean density differences (Largier 2020). While not all quantities can be estimated with the existing data over the period of interest, and it is likely that forcing terms may vary substantially across different regions of the bay [e.g., due to spatial differences in wind forcing and thermal gradients – see e.g., Largier (2020)], some insight can be gained by generally considering the relative importance of these terms during the two upwelling seasons. During Peak Upwelling, thermal forcing was weakest [see Fig. 10 in Walter et al. (2018) that shows relatively minimal bay-ocean temperature differences at this location during this time of the year, albeit using averages across different years than in the current study], while the average mean wind stress (and hence wind forcing) was largest, although highly variable due to strong upwelling-relaxation cycling [see Fig. 3 in Walter et al. (2018)]. The conditionally averaged flow field displayed larger velocities along the upwelling jet, but also farther offshore in the shelf jet, indicating that slight increases in both wind and shelf jet forcing drove the differences in the conditionally versus traditionally-averaged flow fields. During the Upwelling Relaxation, thermal forcing in the bay was significantly enhanced [see Fig. 10 in Walter et al. (2018)], whereas the relative importance of shelf jet forcing (Fig. 7) and wind forcing [see Fig. 3 in Walter et al. (2018)] were significantly reduced. The conditionally averaged flow field showed enhanced convergence along the mouth, which may be linked with the enhanced thermal forcing and the potential reinforcement of the convergent front. In both the Peak Upwelling and Upwelling Relaxation seasons, shelf jet forcing was enhanced in the conditionally averaged flow field, which with the onshore advection of the upwelling jet, resulted in greater magnitude divergence along the southern portion of the bay near Pt. Sal. Future work (either through modeling and/or appropriately-resolved field--based studies) should consider full momentum balances to properly investigate dynamical balances and the relative importance of different forcing terms spatially.

The small length and shallow depth scales present in small upwelling bays like SLO Bay fit in a dynamical regime in which submesocale

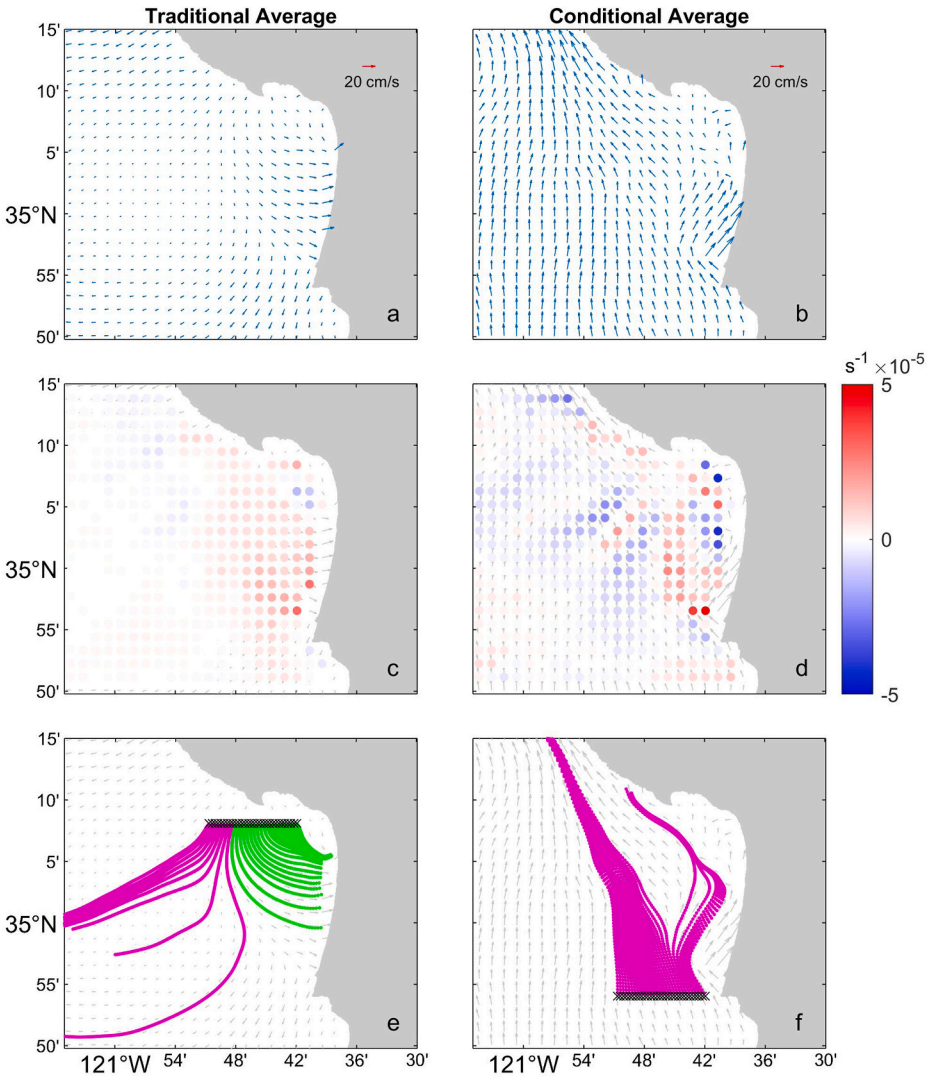

Fig. 10. Same as Fig. 8, but for the Winter Storms season (December, January, and February).

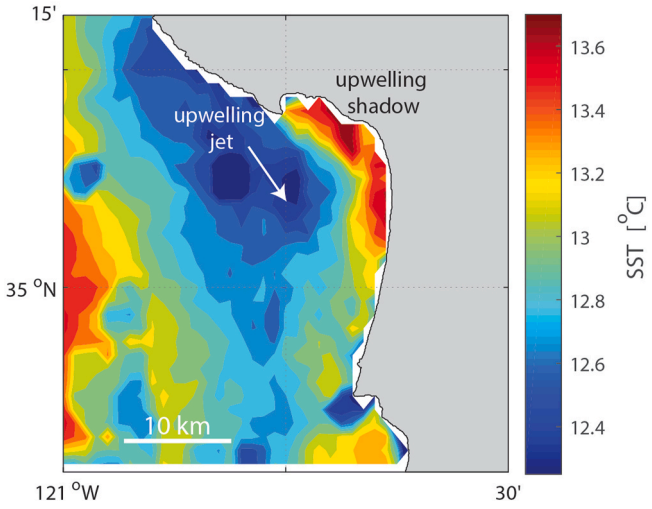

Fig. 11. AVHRR SST highlighting the upwelling jet (blue) and shadow (red). One-month composite from May 2019. (For interpretation of the references to color in this figure legend, the reader is referred to the Web version of this article.)

processes may be important, differing fundamentally from much larger systems like those of Monterey Bay (McWilliams 2016). This is consistent with the horizontal divergence values on the order of the local Coriolis parameter (f) in SLO Bay (i.e., $|\text{divergence}|/f \sim 0.6$ across the bay boundary during the full upwelling season), even at the 2 km spatial resolution of the HFR data. This is in strong contrast to the values observed in Monterey Bay ($|\text{divergence}|/f \sim 0.25$; Paduan et al., 2018). In SLO Bay, the enhanced divergence magnitudes observed in the conditionally averaged fields (particularly the Upwelling Relaxation season) highlights the potential importance of upwelling-driven flows for submesoscale frontal dynamics in small embayments, and by extension, tracer dispersion (Dauhajre et al., 2017). There are few observational studies of submesoscale fronts in coastal regions due to their ephemeral nature, but small upwelling bays downstream of headlands may be sites of consistent front formation, differing fundamentally from larger systems like Monterey Bay, and warrant further study (Dauhajre et al., 2017).

4.3. Ecological ramifications

In upwelling shadow systems, there is an increased potential for local recruitment that is attributed to strong retention in these systems (Largier, 2020). Interestingly, during the Peak Upwelling season, the traditionally averaged flow field showed an increase in particle transport into

the bay relative to the conditionally averaged flow field, whereas there was no appreciable difference over the Upwelling Relaxation and full upwelling seasons. This suggests that the strong divergence that develops in the southern end of the bay in the conditionally averaged flow field during strong upwelling forcing could potentially decrease larval transport and dispersal into the bay. While surface flows can increase (or as shown in the Peak Upwelling season can decrease) plankton transport into the bay, the upwelling front (identified by the regions of enhanced convergence) can also act as a barrier to dispersal and exchange. Surface convergence can aggregate plankton (and other material), and enhanced stratification in the upwelling shadow can create conditions conducive for a local "bloom incubator" (Ryan et al. 2008a, 2008b), thereby increasing the risk of HABs and respiration-driven hypoxia (Barth et al., 2020; Valera et al., 2020). This risk is greatest in SLO Bay during the Upwelling Relaxation season, when local conditions are favorable for dinoflagellate blooms and hypoxic events (Barth et al., 2020; Valera et al., 2020). During the Upwelling Relaxation season, the convergence region across the mouth of the bay is significantly enhanced in the conditionally averaged flow field relative to the traditionally averaged flow field, suggesting that upwelling-driven circulation may actually increase the risk for HABs and hypoxia during this season.

During downwelling events, the poleward flows observed in the conditionally averaged flow fields are in sharp contrast to the equatorward flows in the traditionally averaged flow fields across all non-upwelling seasons. The poleward flows may provide an opportunity for species that have planktonic larval stages to expand their range poleward. It is possible that the bay may serve as a "stepping stone" refuge for poleward expanding species during downwelling (and relaxation, e.g., Washburn et al., 2011) events, given the proximity to Point Conception (~80 km to south), a major marine biogeographic divide (Blanchette et al., 2007). These ideas reinforce the importance of intraseasonal variability in upwelling- and downwelling-driven circulation in shaping nearshore ecology and the idea that temporally averaged flow fields may not accurately predict connectivity patterns and larval transport (see also Nidzieko and Largier, 2013).

5. Conclusion

We apply a conditional averaging technique to investigate intraseasonal differences in upwelling- and downwelling-driven circulation in a small coastal embayment. This is also the first study to investigate seasonal patterns in surface currents in and around SLO Bay. Conditional averaging reveals distinct intraseasonal differences and features that are obscured by traditional seasonal averages when examining the upwelling jet separation and onshore advection, horizontal divergence patterns, and particle trajectories. We show that the upwelling circulation and resulting upwelling jet separation and onshore advection reinforce a convergent upwelling shadow front at this site, with important ecological ramifications. While tuned specifically for SLO Bay, these findings can be used as a baseline for similar small upwelling bays and highlight the importance of conditional averages (versus traditional temporal averages) and coastal upwelling seasonality beyond the bimodal upwelling and non-upwelling description.

Declaration of competing interest

The authors declare that they have no known competing financial interests or personal relationships that could have appeared to influence the work reported in this paper.

Data availability

Data are publicly available (URL in paper)

Acknowledgements

We acknowledge support from the NOAA IOOS program through SCCOOS for the HF radar measurements, as well as past PIs and technicians that helped maintain these systems, especially Ian Robbins. We also acknowledge helpful exchanges with Mike Cook, Tom Connolly, and Piero Mazzini. Comments and suggestions from two anonymous reviewers improved this manuscript.

References

Barth, Alex, Walter, Ryan, Robbins, Ian, Pasulka, Alexis, 2020. Seasonal and interannual variability of phytoplankton abundance and community composition on the Central Coast of California. Mar. Ecol. Progr. Ser. 637, 29–43. https://doi.org/10.3354/meps13245.

Blanchette, C.A., Helmuth, B., Gaines, S.D., 2007. Spatial patterns of growth in the mussel, Mytilus californianus, across a major oceanographic and biogeographic boundary at Point Conception, California, USA. J. Exp. Mar. Biol. Ecol. 340, 126–148. https://doi.org/10.1016/j.jembe.2006.09.022.

Checkley, D.M., Barth, J.A., 2009. Patterns and processes in the California current system. Progress in Oceanography 83, 49–64. https://doi.org/10.1016/j.pocean.2009.07.028.

Coulliette, C., Lekien, F., Paduan, J.D., Haller, G., Marsden, J.E., 2007. Optimal pollution mitigation in Monterey bay based on coastal radar data and nonlinear dynamics. Environ. Sci. Technol. 41, 6562–6572. https://doi.org/10.1021/es0630691.

Dauhajre, D.P., McWilliams, J.C., Uchiyama, Y., 2017. Submesoscale coherent structures on the continental shelf. Journal of Physical Oceanography 47, 2949–2976. https://doi.org/10.1175/JPO-D-16-0270.1.

García-Reyes, M., Largier, J.L., 2012. Seasonality of coastal upwelling off central and northern California: new insights, including temporal and spatial variability. J. Geophys. Res. 117 https://doi.org/10.1029/2011JC007629 n/a-n/a.

Kim, S.Y., Terill, E.J., Cornuelle, B.D., 2009. Assessing coastal plumes in a region of multiple discharges: the US-Mexico border. Environ. Sci. Technol. 43, 7450–7457. https://doi.org/10.1021/es900775p.

Largier, J.L., 2020. Upwelling bays: how coastal upwelling controls circulation, habitat, and productivity in bays. Annu. Rev. Mar. Sci. 12, 415–447. https://doi.org/10.1146/annurev-marine-010419-011020.

Matson, P.G., Washburn, L., Fields, E.A., Gotschalk, C., Ladd, T.M., Siegel, D.A., Welch, Z.S., Iglesias-Rodriguez, M.D., 2019. Formation, development, and propagation of a rare coastal coccolithophore bloom. J. Geophys. Res. Oceans 124, 3298–3316. https://doi.org/10.1029/2019JC015072.

McWilliams, J.C., 2016. Submesoscale currents in the ocean. Proc. R. Soc. A. 472, 20160117. https://doi.org/10.1098/rspa.2016.0117.

Moraga-Opazo, J., Valle-Levinson, A., Ramos, M., Pizarro-Koch, M., 2011. Upwelling-triggered near-geostrophic recirculation in an equatorward facing embayment. Continental Shelf Research 31, 1991–1999. https://doi.org/10.1016/j.csr.2011.10.002.

Nidzieko, N.J., Largier, J.L., 2013. Inner shelf intrusions of offshore water in an upwelling system affect coastal connectivity. Geophys. Res. Lett. 40, 5423–5428. https://doi.org/10.1002/2013GL056756.

Paduan, J.D., Washburn, L., 2013. High-frequency radar observations of ocean surface currents. Annu. Rev. Mar. Sci. 5, 115–136. https://doi.org/10.1146/annurev-marine-121211-172315.

Paduan, J.D., Cook, M.S., Tapia, V.M., 2018. Patterns of upwelling and relaxation around Monterey Bay based on long-term observations of surface currents from high frequency radar. Deep Sea Research Part II: Topical Studies in Oceanography 151, 129–136. https://doi.org/10.1016/j.dsr2.2016.10.007.

Roughan, M., Terrill, E.J., Largier, J.L., Otero, M.P., 2005a. Observations of divergence and upwelling around Point Loma, California. J. Geophys. Res. 110, C04011. https://doi.org/10.1029/2004JC002662.

Roughan, M., Mace, A.J., Largier, J.L., Morgan, S.G., Fisher, J.L., Carter, M.L., 2005b. Subsurface recirculation and larval retention in the lee of a small headland: a variation on the upwelling shadow theme. J. Geophys. Res. 110, C10027. https://doi.org/10.1029/2005JC002898.

Ryan, J., McManus, M., Paduan, J., Chavez, F., 2008a. Phytoplankton thin layers caused by shear in frontal zones of a coastal upwelling system. Mar. Ecol. Prog. Ser. 354, 21–34. https://doi.org/10.3354/meps07222.

Ryan, J.P., Gower, J.F.R., King, S.A., Bissett, W.P., Fischer, A.M., Kudela, R.M., Kolber, Z., Mazzillo, F., Rienecker, E.V., Chavez, F.P., 2008b. A coastal ocean extreme bloom incubator. Geophys. Res. Lett. 35 https://doi.org/10.1029/2008GL034081 n/a-n/a.

Valera, M., Walter, R.K., Bailey, B.A., Castillo, J.E., 2020. Machine learning based predictions of dissolved oxygen in a small coastal embayment. JMSE 8, 1007. https://doi.org/10.3390/jmse8121007.

Valle-Levinson, A., Moraga, J., Olivares, J., Blanco, J.L., 2000. Tidal and residual circulation in a semi-arid bay: coquimbo Bay, Chile. Continental Shelf Research 20, 2009–2028. https://doi.org/10.1016/S0278-4343(00)00060-1.

Valle–Levinson, A., Schneider, W., Sobarzo, M., Bello, M., Bravo, L., Castillo, M., Duarte, L., Fuenzalida, R., Gallegos, J.M., Garcés–Vargas, J., González, J., Gutiérrez, D., Molinet, C., Navarro, M.S., Pierini, J., Rodríguez–Rubio, E., Valdenegro, A., Vera, L., Zenteno, L., 2004. Wind-induced exchange at the entrance to Concepción Bay, an equatorward facing embayment in central Chile. Deep Sea

Research Part II: Topical Studies in Oceanography 51, 2371–2388. https://doi.org/10.1016/j.dsr2.2004.08.010.

Walter, R.K., Stastna, M., Woodson, C.B., Monismith, S.G., 2016. Observations of nonlinear internal waves at a persistent coastal upwelling front. Continental Shelf Research 117, 100–117. https://doi.org/10.1016/j.csr.2016.02.007.

Walter, R.K., Reid, E.C., Davis, K.A., Armenta, K.J., Merhoff, K., Nidzieko, N.J., 2017. Local diurnal wind-driven variability and upwelling in a small coastal embayment. J. Geophys. Res. Oceans 122, 955–972. https://doi.org/10.1002/2016JC012466.

Walter, R.K., Armenta, K.J., Shearer, B., Robbins, I., Steinbeck, J., 2018. Coastal upwelling seasonality and variability of temperature and chlorophyll in a small coastal embayment. Continental Shelf Research 154, 9–18. https://doi.org/10.1016/j.csr.2018.01.002.

Warrick, J.A., DiGiacomo, P.M., Weisberg, S.B., Nezlin, N.P., Mengel, M., Jones, B.H., Ohlmann, J.C., Washburn, L., Terrill, E.J., Farnsworth, K.L., 2007. River plume patterns and processes within the Southern California Bight. Continental Shelf Research 27, 2427–2448. https://doi.org/10.1016/j.csr.2007.06.015.

Washburn, L., Fewings, M.R., Melton, C., Gotschalk, C., 2011. The propagating response of coastal circulation due to wind relaxations along the central California coast. J. Geophys. Res. 116, C12028. https://doi.org/10.1029/2011JC007502.

Woodson, C.B., Eerkes-Medrano, D.I., Flores-Morales, A., Foley, M.M., Henkel, S.K., Hessing-Lewis, M., Jacinto, D., Needles, L., Nishizaki, M.T., O'Leary, J., Ostrander, C.E., Pespeni, M., Schwager, K.B., Tyburczy, J.A., Weersing, K.A., Kirincich, A.R., Barth, J.A., McManus, M.A., Washburn, L., 2007. Local diurnal upwelling driven by sea breezes in northern Monterey Bay. Continental Shelf Research 27, 2289–2302. https://doi.org/10.1016/j.csr.2007.05.014.

Woodson, C.B., Washburn, L., Barth, J.A., Hoover, D.J., Kirincich, A.R., McManus, M.A., Ryan, J.P., Tyburczy, J., 2009. Northern Monterey Bay upwelling shadow front: observations of a coastally and surface-trapped buoyant plume. J. Geophys. Res. 114, C12013. https://doi.org/10.1029/2009JC005623.

Zelenke, B., Moline, M.A., Crawford, G.B., Garfield, N., Jones, B.H., Largier, J.L., Paduan, J.D., Ramp, S.R., Terrill, E.J., Washburn, L., 2009. Evaluating connectivity between marine protected areas using CODAR high-frequency radar. In: OCEANS 2009. Presented at the OCEANS 2009. IEEE, Biloxi, MS, pp. 1–10. https://doi.org/10.23919/OCEANS.2009.5422272.